

Overcoming resistance to HER2 inhibitors through state-specific kinase binding

Chris J Novotny^{1,2}, Sirkku Pollari³, Jin H Park^{4,5}, Mark A Lemmon⁴⁻⁶, Weijun Shen^{3*} & Kevan M Shokat^{1,2*}

The heterodimeric receptor tyrosine kinase complex formed by HER2 and HER3 can act as an oncogenic driver and is also responsible for rescuing a large number of cancers from a diverse set of targeted therapies. Inhibitors of these proteins, particularly HER2, have dramatically improved patient outcomes in the clinic, but recent studies have demonstrated that stimulating the heterodimeric complex, either via growth factors or by increasing the concentrations of HER2 and HER3 at the membrane, significantly diminishes the activity of the inhibitors. To identify an inhibitor of the active HER2–HER3 oncogenic complex, we developed a panel of Ba/F3 cell lines suitable for ultra-high-throughput screening. Medicinal chemistry on the hit scaffold resulted in a previously uncharacterized inhibitor that acts through preferential inhibition of the active state of HER2 and, as a result, is able to overcome cellular mechanisms of resistance such as growth factors or mutations that stabilize the active form of HER2.

Signaling from the epidermal growth factor receptor (EGFR or HER) family of receptor tyrosine kinases (RTKs) is dependent on a well-orchestrated series of interactions between family members to form either homo- or heterodimers¹⁻³. This dimerization process allows the intracellular kinase domains to form an asymmetric dimer in which the C-terminal domain of the ‘activator’ kinase binds to the N-terminal portion of the ‘receiver’ kinase to stabilize it in an active conformation⁴ (Fig. 1a). The receiver kinase then phosphorylates tyrosine residues on the C-terminal tails of the kinases to recruit and activate downstream signaling components, most notably those involved in pathways that promote growth and survival. Because of this, the improper activation of the EGFR family of kinases, either by mutation or overexpression, is observed in a variety of cancers^{5,6}. Interestingly, cell culture studies suggest that rather than causing escape from the biological mechanism of regulation, oncogenic activation alters the equilibrium between active and inactive states to favor the improper dimerization and activation of these receptors⁷⁻⁹. This dependence on dimerization is particularly evident in HER2-overexpressing breast cancers that are dependent on the presence of HER3 (ref. 10).

Within the EGFR family, HER2 and HER3 are unique. HER3 is classified as a pseudokinase with only residual kinase activity, whereas HER2 has no known activating ligand but is constitutively able to dimerize with other active family members. In this way, HER2 and HER3 together form a functional RTK unit, with HER3 responding to activating ligands such as neuregulin, HER2 providing the intracellular kinase activity, and both intracellular domains providing phosphorylation sites. Additionally, HER2 and HER3 are each other’s preferred heterodimerization partners and also form the most mitogenic complex among all possible EGFR-family dimers¹¹. Because of this codependence, HER3 is equally important for the formation, proliferation, and survival of HER2-overexpressing tumors¹².

HER2 amplification and overexpression is the most well-studied means of oncogenic activation of the HER2–HER3 heterodimer. However, improper signaling can also be caused by secretion of the HER3 ligand neuregulin-1 (NRG), which stimulates HER2–HER3

heterodimers in an autocrine manner, as well as by mutations in HER3 that stabilize and activate heterodimers independently of ligand^{13,14}. In addition, mutations that activate the HER2 kinase domain have also been reported¹⁵⁻¹⁷.

Small-molecule kinase inhibitors such as lapatinib and HER2-targeted antibodies such as ado-trastuzumab emtansine (T-DM1) have been developed to treat these tumors and have shown efficacy against HER2-driven cancers in the clinic^{18,19}. However, recent studies have demonstrated that the presence of NRG induces resistance against currently approved HER2-targeted monotherapies through HER2–HER3 signaling^{20,21}. Additionally, either inhibition of HER2–HER3 signaling at the RTK level or inhibition of the downstream PI3K/Akt pathway releases a negative feedback loop that leads to increased transcription, translation, and membrane localization of HER3 (refs. 22–24). This increase in the abundance of HER3 causes a rebound in HER3 phosphorylation and reactivation of the PI3K/Akt pathway even in the continued presence of inhibitor, indicating that formation of HER2–HER3 heterodimers is crucial for intrinsic cellular resistance to current HER2-targeted therapies²⁵. This severe limitation illustrates why more effective therapies targeting the active HER2–HER3 dimer are needed.

Here we evaluated the ability of existing reversible HER2 inhibitors to inhibit signaling and proliferation in cancer cell lines driven by HER2–HER3 heterodimers activated via various oncogenic mechanisms. Across several cell lines, stabilization of HER2 in the active conformation led to severely diminished activity of both lapatinib and TAK-285. We therefore aimed to identify a novel HER2–HER3 inhibitor that would preferentially target the active state of the heterodimer. Reasoning that a biochemical screen would be unable to capture the relevant cellular conformation of the fully formed transmembrane complex, we turned to a cell-based screening strategy. A high-throughput screen of 950,000 small molecules against an engineered Ba/F3 cell line dependent on NRG-stimulated HER2–HER3 heterodimers yielded a hit scaffold that we optimized to create a next-generation HER2 inhibitor. The optimized inhibitor is capable of

¹Howard Hughes Medical Institute, University of California San Francisco, San Francisco, California, USA. ²Department of Cellular and Molecular Pharmacology, University of California San Francisco, San Francisco, California, USA. ³California Institute for Biomedical Research (Calibr), La Jolla, California, USA. ⁴Department of Biochemistry and Biophysics, University of Pennsylvania Perelman School of Medicine, Philadelphia, Pennsylvania, USA.

⁵Graduate Group in Biochemistry and Molecular Biophysics, University of Pennsylvania Perelman School of Medicine, Philadelphia, Pennsylvania, USA.

⁶Present address: Department of Pharmacology and Cancer Biology Institute, Yale University, New Haven, Connecticut, USA.

*e-mail: kevan.shokat@ucsf.edu or wshen@calibr.org

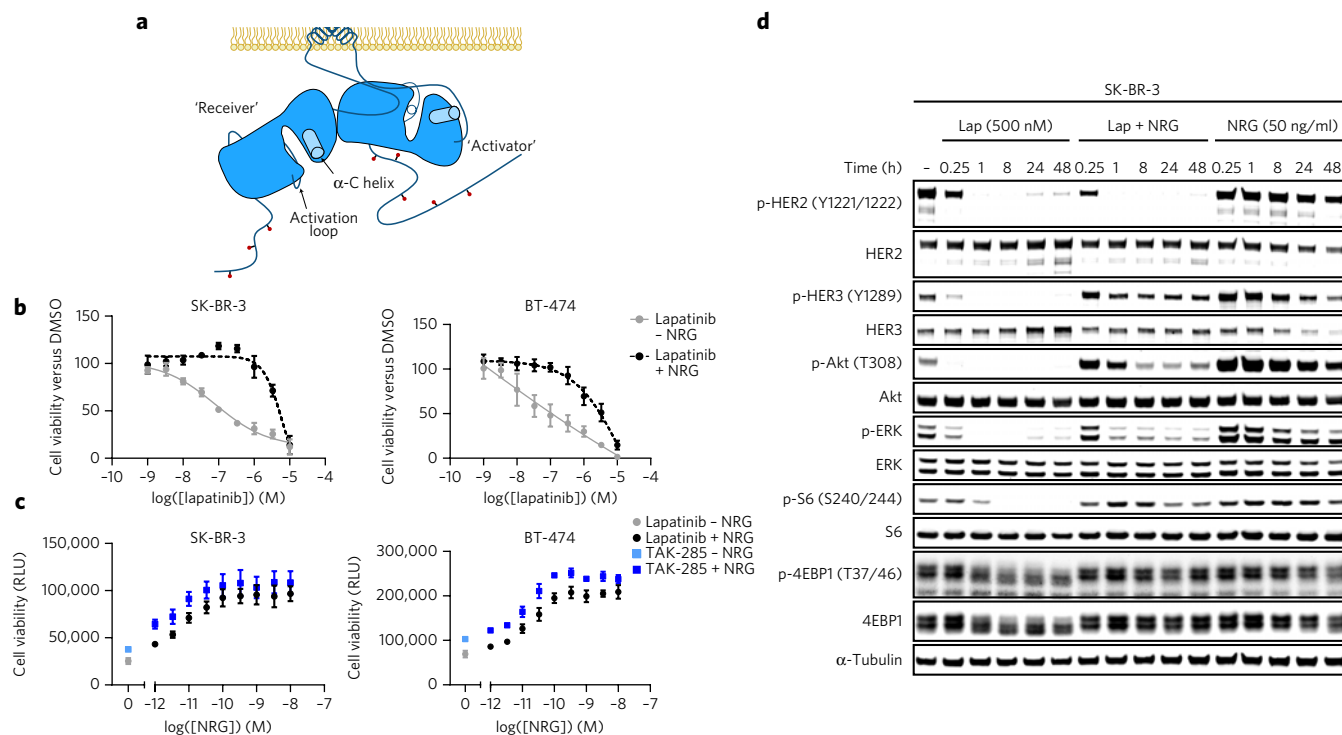


Figure 1 | NRG rescues HER2-overexpressing cancer cells from HER2 inhibitors. (a) The asymmetric dimer of EGFR-family kinase domains. The C-terminal domain of the 'activator' kinase (right) interacts with the N-terminal portion of the 'receiver' kinase (left). This interaction stabilizes the active conformation of the receiver kinase, identified by the 'in' conformation of the receiver kinase's α -C helix and the ordered extension of the activation loop. The activator kinase retains the inactive conformation. (b) Proliferation of SK-BR-3 and BT-474 cells treated with the indicated doses of lapatinib in the presence or absence of NRG. Proliferation was read out after 72 h and normalized to a DMSO control (mean \pm s.d.; $n = 3$). (c) The ability of NRG to rescue SK-BR-3 and BT-474 cell proliferation from HER2 inhibitors is dose dependent. Cells were treated with the indicated inhibitor (1 μ M) in the presence of various concentrations of NRG, and proliferation was read out after 72 h (mean \pm s.d.; $n = 3$). RLU, relative light units (CellTiter-Glo assay). (d) Time course of HER2-HER3 signaling in SK-BR-3 cells treated with either lapatinib (Lap) or NRG, or with both. The addition of NRG rescued p-HER3 and all downstream signaling at all time points examined (full gels shown in **Supplementary Fig. 2**).

potently inhibiting signaling from the HER2-HER3 heterodimer regardless of the activating oncogenic mechanism.

RESULTS

HER2-HER3 heterodimers are resistant to current inhibitors

We first confirmed that the addition of the HER3-activating ligand NRG dramatically rescues the proliferation of HER2-overexpressing breast cancer cell lines treated with the HER2 kinase inhibitors lapatinib and TAK-285 (**Fig. 1b**, **Supplementary Results**, **Supplementary Fig. 1**). This rescue of cell proliferation was dose dependent and was effective with picomolar concentrations of NRG in the presence of either HER2 inhibitor at 1 μ M (**Fig. 1c**). To determine how NRG was able to so profoundly rescue cellular proliferation, we examined a time course of HER2-HER3 signaling in SK-BR-3 cells exposed to either lapatinib or NRG, or to both. Although lapatinib alone rapidly and sustainably inhibited all signaling from HER2 and HER3, the addition of NRG prevented the complete inhibition of phosphorylated HER3 (p-HER3) and all downstream signaling pathways at all time points examined (**Fig. 1d**). Analysis of signaling from alternative EGFR family members that could potentially contribute to this phenotype revealed that EGFR phosphorylation actually decreased in response to NRG and was still inhibited by lapatinib, while HER4, which is thought to function as a tumor suppressor, was undetectable in this cell line^{26,27} (**Supplementary Fig. 3**).

There are several possible mechanisms for NRG's rescue of HER3 signaling in the presence of lapatinib. The very weak kinase activity of HER3 itself is unlikely to be sufficient for signaling,

although it is not inhibited by lapatinib. A more likely explanation for this rescue is that NRG-induced heterodimerization of HER2 and HER3 stabilizes a conformation of the HER2 kinase domain that is resistant to the inhibitors tested. Both lapatinib and TAK-285 occupy a back hydrophobic pocket of HER2 that is available only when the kinase domain is in an inactive conformation with the α -C helix in the characteristic 'out' position; thus, both inhibitors bind only to the kinase conformation described as 'DFG in/ α -C out'^{28,29}. This mode of binding has the advantage of giving these inhibitors slow off-rates but could also explain their ineffectiveness in the presence of NRG. Crystal structures of EGFR-family homodimers and of a HER3-EGFR kinase complex have shown that only the activator kinase in the asymmetric dimer can retain the inactive conformation^{30,31} (**Fig. 1a**). In HER2-HER3 complexes, HER3 can be expected to adopt this position exclusively, whereas HER2 will take the receiver-kinase position and become stabilized in the active conformation. Thus, in a HER2-HER3 complex, the size and accessibility of the back hydrophobic pocket of the HER2 kinase domain will be greatly reduced, preventing lapatinib or TAK-285 from binding.

To determine whether NRG-induced heterodimerization prevents lapatinib binding, we treated serum-starved SK-BR-3 cells with lapatinib either 15 min before or simultaneously with NRG stimulation and then rapidly examined HER2-HER3 signaling to monitor the on-rate of lapatinib in these cells. Lapatinib concentrations greater than 100 nM were sufficient to inhibit the entire RTK signaling pathway when added before NRG (**Fig. 2a**)—that is, in the absence of HER2-HER3 heterodimers. By contrast, lapatinib

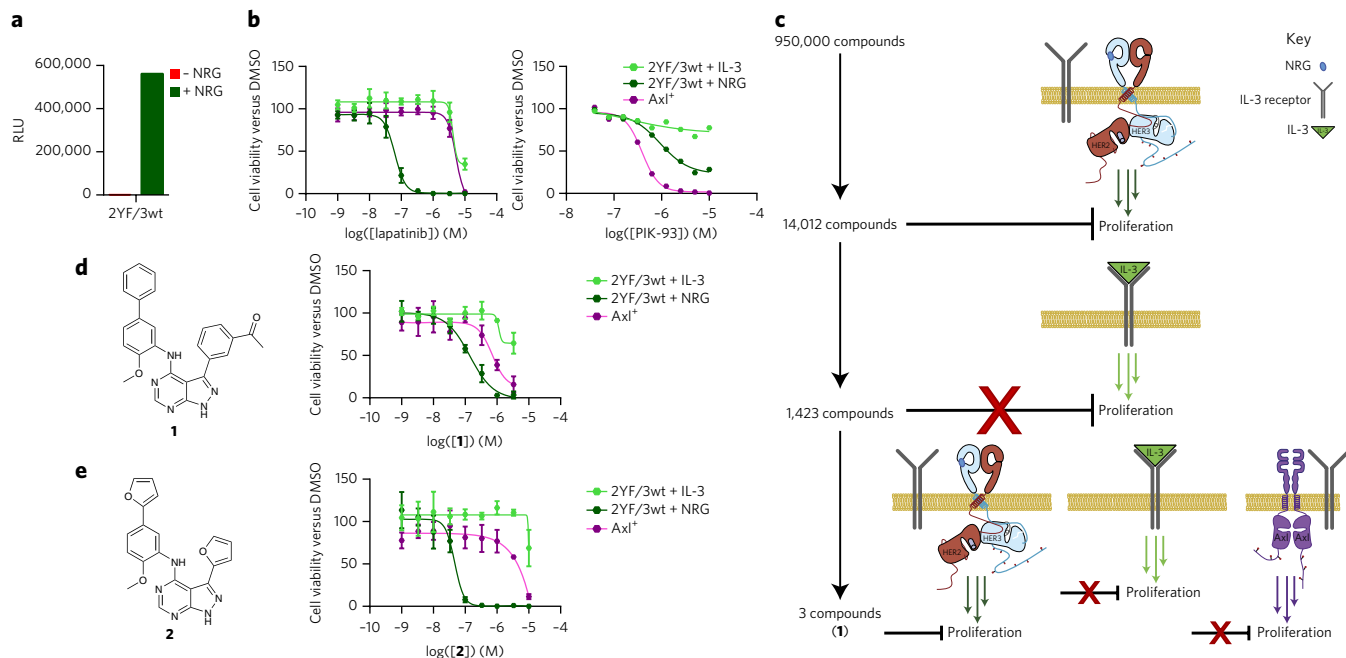


Figure 3 | Design and execution of a high-throughput screen identifies a novel HER2-HER3 inhibitor. (a) 2YF/3wt cells were incubated in the presence or absence of NRG and proliferation was assessed after 48 h (mean, $n = 1$). RLU, relative light units (CellTiter-Glo assay). (b) Assays of Ba/F3 cell viability can distinguish compounds that specifically inhibit signaling at the HER2-HER3 level (lapatinib) from those that hit downstream (PIK-93). Results were read out after 48 h and normalized to a DMSO control (mean \pm s.d.; $n = 3$ for lapatinib and $n = 1$ for PIK-93). (c) Schematic of the high-throughput screen. Compounds were first screened for their ability to inhibit the proliferation of 2YF/3wt cells in the presence of NRG, then counter-screened against the parental cells in the presence of IL-3, and finally screened in dose-response experiments with all three cell lines. (d,e) Compound structures and proliferation curves for **1** and **2** against the panel of Ba/F3 cell lines (mean \pm s.d.; $n = 3$).

rescue signaling and proliferation^{22,23,25}. Our findings therefore suggest that inhibitors that target the active HER2-HER3 heterodimer will have significant advantages, especially in situations that increase the number of active HER2-HER3 heterodimers.

Identification of a novel HER2-HER3 inhibitor

In order to find a small-molecule inhibitor capable of binding to the active HER2-HER3 signaling complex, we developed a high-throughput cellular screen using a Ba/F3 cell line engineered to be dependent on NRG-induced HER2-HER3 heterodimers. Ba/F3 cells are normally dependent on IL-3 signaling for their proliferation and survival but can be made dependent on introduced oncogenic signals³². We sequentially selected transduced Ba/F3 cells for populations stably expressing HER3 and then HER2. To ensure that all of the proliferative signal could be attributed to HER2-HER3 heterodimers rather than HER2 homodimers, the nine C-terminal tyrosines in HER2 were mutated to phenylalanine (HER2YF). We then withdrew IL-3 and supplemented the media with NRG to select for NRG-dependent cells expressing HER2YF and wild-type HER3 (2YF/3wt). The resulting 2YF/3wt cell line was completely dependent on NRG for survival and allowed us to screen for inhibitors of full-length HER2-HER3 heterodimers in their native cellular conformations using a cell-viability assay (Fig. 3a). In addition to allowing us to identify potential inhibitors of active HER2, this cellular system also has the potential to uncover compounds with novel mechanisms of action against the pseudokinase HER3.

We sought to validate the screen and test the effectiveness of counter-screening with either the same 2YF/3wt Ba/F3 cell line or the parental Ba/F3 cell line in the presence of IL-3 to remove cytotoxic primary hits. Therefore, we first tested a panel of kinase inhibitors with established mechanisms of action. We found that MAPK pathway inhibitors (e.g., vemurafenib) did not score as hits in NRG-treated 2YF/3wt cells, whereas mTOR inhibitors (e.g., MLN0128)

were ruled out in our toxicity counter-screen, showing equal activity in the presence of either NRG or IL-3 (Supplementary Fig. 6). By contrast, HER2 and PI3K inhibitors showed selective inhibition of NRG-driven cells over IL-3-driven cells (Fig. 3b). In order to rapidly remove any hit compound that did not directly target the HER2-HER3 heterodimer, we created a separate Ba/F3 cell line dependent on the overexpression of full-length wild-type Axl, another RTK that signals through the PI3K pathway. This panel of Ba/F3 cell lines was able to distinguish lapatinib from the PI3K inhibitor PIK-93 (Fig. 3b).

The 48-h proliferation assay of 2YF/3wt cells in the presence of NRG was miniaturized and optimized for 1,536-well plates, which we used to screen a diverse collection of 950,000 drug-like molecules ($Z' \geq 0.75$). This primary screen resulted in 14,012 hits (>50% inhibition compared with a DMSO control), which were reduced to 1,423 compounds after triplicate confirmation and the counter-screen using parental Ba/F3 cells in the presence of IL-3 (<30% inhibition versus DMSO). These 1,423 compounds were then assayed in dose-response experiments with all three cell lines (2YF/3wt plus NRG, parental Ba/F3 plus IL-3, and Axl⁺; Fig. 3c and Supplementary Table 1). This screening and triaging process led to the identification of three hit compounds sharing the same scaffold, exemplified by compound **1** (Fig. 3d), which reproducibly showed preferential inhibition of 2YF/3wt cell proliferation in the presence of NRG. Optimization of the hit scaffold through five iterations of analog synthesis, each consisting of approximately ten compounds, produced compound **2**, which showed a marked preference for inhibition of the NRG-driven cells over the others (Fig. 3e).

The cellular activity of **2** results from HER2 inhibition

The specificity of **2** for the NRG-driven 2YF/3wt cells indicated that the compound had reasonable kinase specificity and was probably interfering with signaling at the RTK level. This was confirmed by

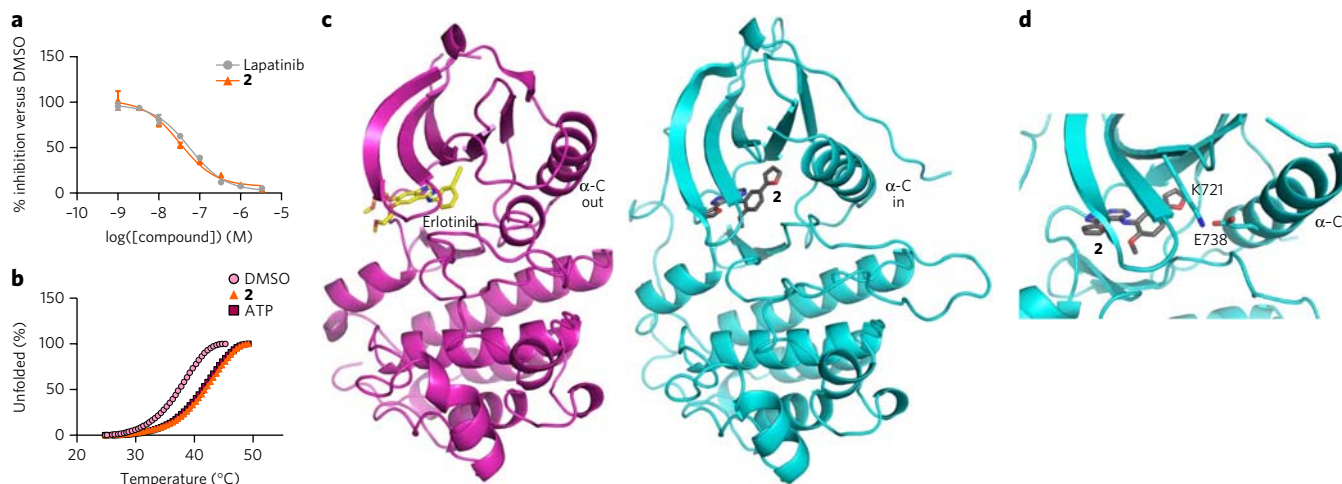


Figure 4 | Compound 2 is a selective type I inhibitor of HER2. (a) *In vitro* kinase assay of the HER2 kinase domain against lapatinib and **2** (mean \pm s.d.; $n = 3$). (b) Thermal stabilization of the HER3 kinase domain by either **2** or ATP as determined by thermofluor assay (mean; $n = 2$). (c) The crystal structures of erlotinib (left; PDB 4HJO) and **2** (right) bound to EGFR TKD V924R. Despite the inactivating mutation, the kinase domain in complex with **2** is stabilized in the active conformation by drug binding, as evidenced by the ordered extension of the activation loop and the inward positioning of the α -C helix. (d) Magnified view of the EGFR TKD V924R active site when bound to **2** showing the proximity of the β 3 lysine (K721) and the glutamate (E738) in the α -C helix, which are positioned so as to make a predicted salt bridge.

in vitro profiling against a panel of kinases, with **2** potently inhibiting only EGFR and Abl (Supplementary Tables 2 and 3). To determine the mechanism of action of **2**, we evaluated its ability to interact with HER2 and HER3 using an *in vitro* kinase assay and thermofluor, respectively. Compound **2** was equipotent to lapatinib against HER2 *in vitro* (Fig. 4a) and, surprisingly, was also capable of binding to HER3 (Fig. 4b). Moreover, unlike all other EGFR-family inhibitors examined so far, **2** was also able to inhibit the small amount of HER3 autophosphorylation seen when the purified HER3 intracellular domain is clustered, indicating that it binds to the HER3 active site (Supplementary Fig. 7).

To determine how **2** is able to interact with multiple members of the EGFR family, we determined the X-ray crystal structure of **2** bound to the EGFR tyrosine kinase domain (Fig. 4c and Supplementary Table 4). Although crystals were obtained with both the wild-type kinase domain and a V924R-mutated variant, the latter (EGFR TKD V924R) was optimized most readily. The V924R kinase domain crystallizes in the inactive (autoinhibited) conformation in the absence of inhibitor or when bound to the type I EGFR inhibitor erlotinib, because this mutation places a polar arginine side chain in the middle of the hydrophobic patch used to form the asymmetric dimer required for EGFR dimerization^{33,34} (Fig. 4c). Strikingly, **2** stabilized the active conformation of this mutated EGFR kinase domain in crystals without forming the characteristic asymmetric dimer, as evidenced by the ordered extension of the activation loop as well as by the 'in' conformation of the α -C helix, which allows formation of the characteristic salt bridge between the β 3 lysine and the α -C glutamate (Fig. 4c,d). This finding indicates that our hit scaffold may have a strong preference for binding and stabilizing the active conformation of EGFR-family kinase domains. Interestingly, the HER3 kinase domain has only ever been crystallized in the inactive conformation, and it did not crystallize after the introduction of mutations designed to destabilize the inactive state or in the presence of **2** (refs. 35,36). This suggests that **2** may stabilize an alternative HER3 kinase domain conformation that could potentially prevent HER3 from allosterically activating HER2.

To determine whether binding to HER2, HER3, or both was responsible for the antiproliferative activity of **2**, we created a series of Ba/F3 cell lines dependent on NRG-induced HER2–HER3 heterodimers that possessed methionine gatekeeper mutations (TM) in either kinase alone (2YF/3TM and 2YFTM/HER3wt) or in

both (2YFTM/3TM). The methionine gatekeeper mutation has been shown to prevent lapatinib from binding to HER2 (ref. 37), and it reduced the ability of **2** to bind to either kinase in isolation (Supplementary Fig. 8). Consistent with previous reports, both lapatinib and gefitinib (an EGFR inhibitor capable of inhibiting HER2 to a lesser extent) were unable to inhibit the proliferation of either Ba/F3 cell line that contained the gatekeeper mutation in HER2. Similarly, inhibition by **2** was affected only by the HER2 gatekeeper mutation, whereas the gatekeeper mutation in HER3 had little influence (Supplementary Table 5). These data indicate that the cellular activity of **2** is due to inhibition of HER2 kinase activity.

Type I HER2 inhibitors are insensitive to NRG stimulation

Reasoning that a type I inhibitor of HER2 could possess the necessary attributes to inhibit signaling from the active HER2–HER3 heterodimer, we set out to further optimize the potency of our inhibitor. The crystal structure suggested that the extra-cyclic NH linker could form an intramolecular hydrogen bond with the 2-furan, which would help to stabilize the inhibitor in a conformation necessary for binding to the active kinase. The structure also suggested that limiting the charge density on the other 2-furan ring would prevent negative interactions with the kinase. With these parameters in mind, we undertook a second optimization effort; this led to compound **3**, which showed superior activity to lapatinib in 2YF/3wt cells in the presence of NRG, as well as specificity for this cell line over the others by multiple orders of magnitude (Fig. 5a,b). *In vitro* kinase profiling of **3** revealed a similar profile to **2** as well as similar potency against HER2 (Supplementary Table 6 and Supplementary Fig. 9).

Consistent with our hypothesis that a potent type I inhibitor of HER2 would be unaffected by the presence of NRG, **3** showed little to no shift in its ability to inhibit the growth and signaling of HER2-overexpressing cell lines in the presence of NRG (Fig. 5c and Supplementary Fig. 10). Additionally, unlike lapatinib and TAK-285, 1 μ M **3** was able to inhibit the proliferation of HER2-overexpressing cells over a range of NRG concentrations and was also able to induce cell death in the presence of NRG (Supplementary Fig. 11). To confirm that **3** could bind to the actively signaling HER2–HER3 heterodimer, we looked at signaling 15 min after the addition of NRG in SK-BR-3 cells either pretreated with **3** and then stimulated by NRG, or simultaneously treated with **3** and NRG. The minimal influence of NRG on the ability of

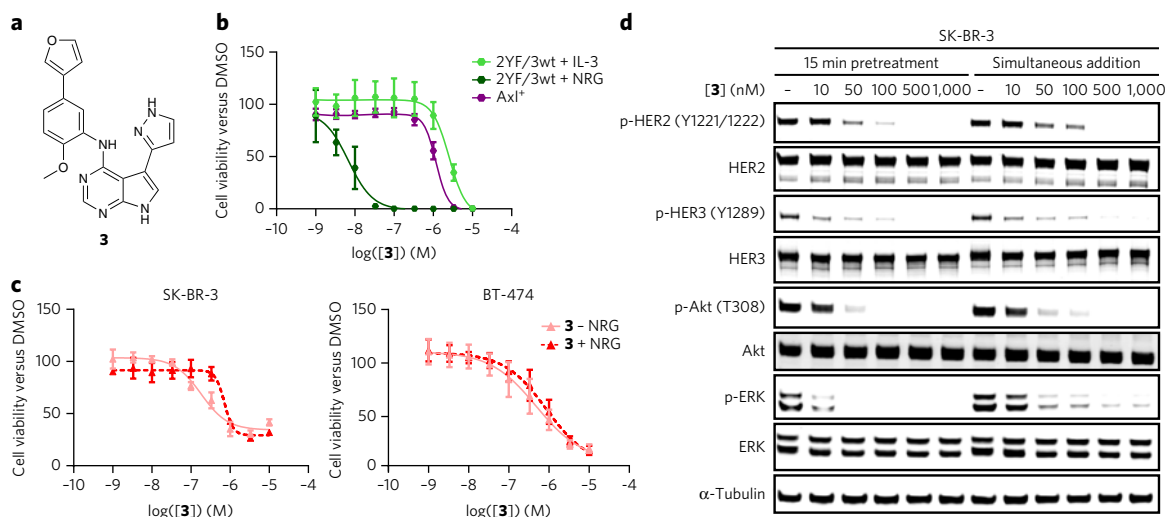


Figure 5 | A type I inhibitor of HER2 is insensitive to the presence of NRG. (a) Chemical structure of **3**. (b) Proliferation curves for the Ba/F3 cell line panel with various concentrations of **3** (mean \pm s.d.; $n = 3$). (c) Proliferation of SK-BR-3 and BT-474 cells treated with the indicated doses of **3** in the presence or absence of NRG, showing that **3** is insensitive to the presence of NRG in HER2-overexpressing cell lines (mean \pm s.d.; $n = 3$). Proliferation in **b** and **c** was read out after 72 h and normalized to a DMSO control. (d) Results of the assay described in **Figure 2a** performed with **3** in SK-BR-3 cells (full gels shown in **Supplementary Fig. 12**).

3 to inhibit all levels of signaling, with or without preincubation, especially compared with lapatinib (compare **Fig. 5d** to **Fig. 2a**), suggested that it is capable of binding to and inhibiting the active HER2–HER3 complex, which is not disrupted by **3** (**Fig. 5d** and **Supplementary Fig. 13**). A similar result was obtained in non-HER2-amplified MCF-7 cells and when NRG or vehicle was added before various concentrations of **3** (**Supplementary Figs. 14** and **15**).

Consistent with the results in the HER2-overexpressing cell lines, CW-2 cells were equally sensitive to **3** in the presence or absence of NRG, in both proliferation and signaling assays (**Fig. 6a,b**). This superior activity of **3** compared to that of lapatinib with the CW-2 cells was not due solely to the L755S mutation in HER2, as a similar trend was also seen in a Ba/F3 cell line dependent on a HER3 E928G mutant (2YF/3EG), which can grow independently of NRG (**Supplementary Fig. 17**).

The ability of **3** to inhibit the activated form of HER2 was not limited to growth-factor-induced heterodimers, as **3** rapidly and fully inhibited the mutationally activated form of HER2 in NCI-H1781 cells and thus inhibited their proliferation (**Fig. 6c,d**). To further evaluate the effect of **3** against HER2 mutants within a HER2–HER3 heterodimer, we transduced Ba/F3 cells containing wild-type HER3 with HER2YF constructs carrying reported oncogenic HER2 mutations^{15,16}. The resulting cell lines contained the following HER2 mutations: L755S (2YF-L755S/3wt); duplication of residues Tyr772 to Ala775 (2YF-YVMA/3wt); and an insertion mutation that mutates Gly776 to valine and cysteine (2YF-VC/3wt). These cells remained sensitive to **3** but showed complete resistance to lapatinib (**Supplementary Table 7**).

An additional mechanism by which cancers can become dependent on HER2–HER3 dimers is through NRG-mediated autocrine signaling¹³. Proliferation of the NRG-autocrine-dependent CHL-1 cell line was affected similarly by lapatinib and **3** when measured at 72 h using CellTiter-Glo (**Supplementary Fig. 18a**). However, when we monitored the growth of CHL-1 cells using microscopy, we found that the antiproliferative effect of **3** was more immediate and more potent than that of lapatinib (**Supplementary Fig. 18b**).

We next examined signaling in CHL-1 cells after 24 h of drug treatment and found that **3** was better able to inhibit NRG autocrine signaling in the presence of feedback, as evidenced by the increasing expression of HER2 and HER3 with increasing drug concentration

(**Fig. 6e**). To further examine the differing abilities of **3** and lapatinib to inhibit feedback-released signaling in the NRG autocrine cells, we pretreated CHL-1 cells with lapatinib for 24 h to induce feedback signaling, washed the cells, and then treated them with various concentrations of either lapatinib or **3** for an additional 24 h. Whereas lapatinib inhibited feedback signaling to a lesser extent than the 24-h treatment by itself, there was little to no change in inhibition by **3**, which showed complete inhibition at 1 μ M (**Fig. 6f**). Similar results were obtained in FaDu cells that are also dependent on NRG autocrine signaling (**Supplementary Fig. 19**).

To determine the feasibility of using **3** *in vivo*, we analyzed the pharmacokinetics after either intravenous or intraperitoneal administration in mice (**Supplementary Fig. 20**). The short half-life of the inhibitor precluded a thorough test of **3** against xenografts, and improving the pharmacokinetic properties of the inhibitor scaffold will be a focus of future optimization efforts.

DISCUSSION

The conformational dynamics of protein kinases are critical for their function and for many of the adaptable characteristics of kinase-driven signaling pathways. Particular kinase conformations also offer access to distinctive structural features that can be exploited in the design of inhibitors to gain selectivity even among well-conserved protein families. The DFG-in/ α -C-out binding inhibitor lapatinib targets the inactive state of a kinase with its benzyl ether substituent, which when combined with the quinazoline scaffold grants it exquisite selectivity for the EGFR family of kinases. What has so far been largely unappreciated is the vulnerability of this class of inhibitors to mechanisms that stabilize the active state of the targeted kinases, leading to drug resistance, as we describe here.

Our study highlights this vulnerability and demonstrates that stabilizing the active conformation of HER2 through various mechanisms, including mutations and protein–protein interactions, results in resistance to lapatinib. The challenge is therefore to develop a potent inhibitor of the HER2–HER3 heterodimer whose selectivity is independent of binding to the inactive state. To discover such an inhibitor, we turned to cell-based screening, which has demonstrated a unique capacity to identify novel kinase inhibitors that target the relevant conformation of a protein in its endogenous environment^{38,39}. A screen of close to 1 million small

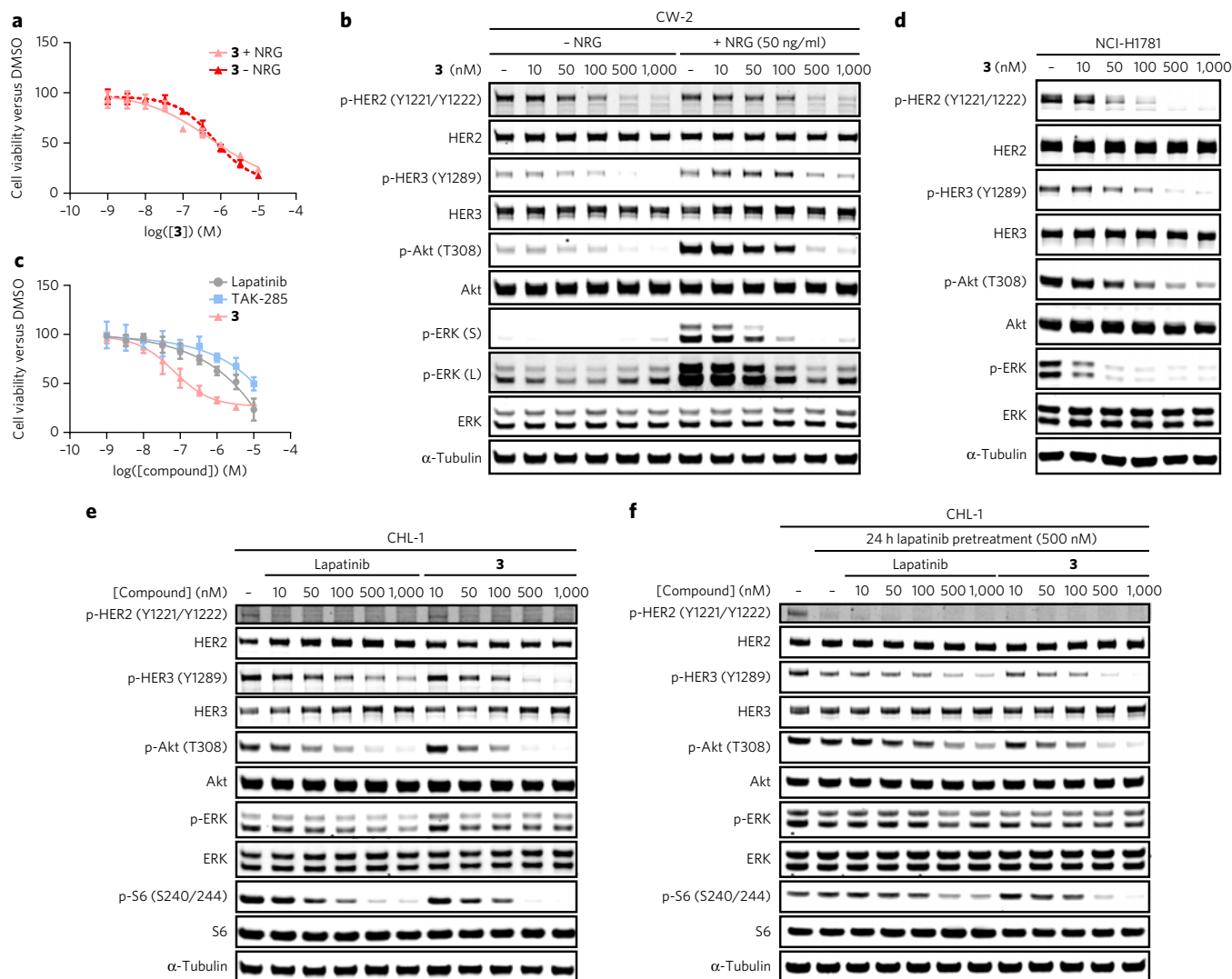


Figure 6 | Compound 3 inhibits the active HER2-HER3 heterodimer in multiple oncogenic settings. (a) Proliferation of CW-2 cells treated with **3** in the presence or absence of NRG (mean \pm s.d.; $n = 3$). (b) Signaling in CW-2 cells treated with the indicated doses of **3** in the presence or absence of NRG (50 ng/ml) for 1 h (full gels shown in **Supplementary Fig. 16a**). (c) Proliferation of NCI-H1781 cells at 72 h (normalized to DMSO control) showing that they were sensitive to **3** but not to DFG-in/ α -C-out inhibitors (mean \pm s.d.; $n = 3$). (d) Signaling in NCI-H1781 cells treated with the indicated doses of **3** and evaluated after 15 min (full gels shown in **Supplementary Fig. 16b**). (e) Signaling in CHL-1 cells treated with the indicated doses of either lapatinib or **3** for 24 h. Compound **3** was better able to inhibit p-HER3 and thus the PI3K/Akt pathway (full gels shown in **Supplementary Fig. 16c**). (f) CHL-1 cells were treated with either DMSO or 500 nM lapatinib for 24 h. The cells were then washed and treated with the indicated doses of either lapatinib or **3** for an additional 24 h. Signaling showed that **3** was better able to inhibit feedback-activated HER2-HER3 signaling in CHL-1 cells (full gels shown in **Supplementary Fig. 16d**).

molecules revealed a novel inhibitor whose potency and selectivity were improved through iterative rounds of medicinal chemistry. The resulting EGFR-family inhibitor has the striking ability to inhibit the mutationally activated form of HER2 as well as NRG-stabilized HER2-HER3 signaling complexes, both of which are insensitive to the clinical inhibitor lapatinib.

Although our approach sought a single agent that could address the challenge of inhibiting the active HER2-HER3 heterodimer, alternative strategies using the HER2-targeting antibody pertuzumab in conjunction with T-DM1 have also been shown to be efficacious. This treatment regimen would require sufficient doses of both drugs to be consistently present, as either agent by itself is unable to inhibit signaling or growth of HER2-driven cells in the presence of NRG²⁰. Additionally, this dual-antibody-based strategy would be unable to target the p95 fragment of HER2, which is associated with trastuzumab resistance^{40,41} and poorer clinical outcomes^{42,43}.

Another potential strategy to target NRG-stimulated HER2-HER3 heterodimers is to use neratinib, an irreversible inhibitor of HER2. However, neratinib is based on the same DFG-in/ α -C-out binding scaffold as lapatinib, so although its electrophilic nature may make it more potent than lapatinib, it would also suffer from a reduced ability to bind to the activated form of HER2.

The past decade has seen an industrialization of kinase-inhibitor discovery using purified protein kinases for both drug development and off-target assessment. In other target classes, such as G-protein-coupled receptors and ion channels, cell-based screens have been the rule rather than the exception and have led to a rich array of state-specific modulators. Our work suggests that cell-based assays designed for kinases offer a powerful screening platform that can lead to a similar diversity in the state specificity of kinase inhibitors. We expect that such state-specific binders will exhibit enhanced therapeutic benefit through potentially novel mechanisms of action.

Received 22 January 2016; accepted 16 June 2016;
published online 5 September 2016

METHODS

Methods and any associated references are available in the [online version of the paper](#).

Accession codes. Coordinates have been deposited with Protein Data Bank under accession code [5JEB](#).

References

- Lemmon, M.A., Schlessinger, J. & Ferguson, K.M. The EGFR family: not so prototypical receptor tyrosine kinases. *Cold Spring Harb. Perspect. Biol.* **6**, a020768 (2014).
- Kovacs, E., Zorn, J.A., Huang, Y., Barros, T. & Kuriyan, J. A structural perspective on the regulation of the epidermal growth factor receptor. *Annu. Rev. Biochem.* **84**, 739–764 (2015).
- Doerner, A., Scheck, R. & Schepartz, A. Growth factor identity is encoded by discrete coiled-coil rotamers in the EGFR juxtamembrane region. *Chem. Biol.* **22**, 776–784 (2015).
- Zhang, X., Gureasko, J., Shen, K., Cole, P.A. & Kuriyan, J. An allosteric mechanism for activation of the kinase domain of epidermal growth factor receptor. *Cell* **125**, 1137–1149 (2006).
- Schneider, M.R. & Yarden, Y. The EGFR-HER2 module: a stem cell approach to understanding a prime target and driver of solid tumors. *Oncogene* **35**, 2949–2960 (2015).
- Yarden, Y. & Sliwkowski, M.X. Untangling the ErbB signalling network. *Nat. Rev. Mol. Cell Biol.* **2**, 127–137 (2001).
- Red Brewer, M. *et al.* Mechanism for activation of mutated epidermal growth factor receptors in lung cancer. *Proc. Natl. Acad. Sci. USA* **110**, E3595–E3604 (2013).
- Wang, Z. *et al.* Mechanistic insights into the activation of oncogenic forms of EGF receptor. *Nat. Struct. Mol. Biol.* **18**, 1388–1393 (2011).
- Foster, S.A. *et al.* Activation mechanism of oncogenic deletion mutations in BRAF, EGFR, and HER2. *Cancer Cell* **29**, 477–493 (2016).
- Lee-Hoeflich, S.T. *et al.* A central role for HER3 in HER2-amplified breast cancer: implications for targeted therapy. *Cancer Res.* **68**, 5878–5887 (2008).
- Tzahar, E. *et al.* A hierarchical network of interreceptor interactions determines signal transduction by Neu differentiation factor/neuregulin and epidermal growth factor. *Mol. Cell Biol.* **16**, 5276–5287 (1996).
- Vaught, D.B. *et al.* HER3 is required for HER2-induced preneoplastic changes to the breast epithelium and tumor formation. *Cancer Res.* **72**, 2672–2682 (2012).
- Jaiswal, B.S. *et al.* Oncogenic ERBB3 mutations in human cancers. *Cancer Cell* **23**, 603–617 (2013).
- Wilson, T.R., Lee, D.Y., Berry, L., Shames, D.S. & Settleman, J. Neuregulin-1-mediated autocrine signaling underlies sensitivity to HER2 kinase inhibitors in a subset of human cancers. *Cancer Cell* **20**, 158–172 (2011).
- Bose, R. *et al.* Activating HER2 mutations in HER2 gene amplification negative breast cancer. *Cancer Discov.* **3**, 224–237 (2013).
- Wang, S.E. *et al.* HER2 kinase domain mutation results in constitutive phosphorylation and activation of HER2 and EGFR and resistance to EGFR tyrosine kinase inhibitors. *Cancer Cell* **10**, 25–38 (2006).
- Greulich, H. *et al.* Functional analysis of receptor tyrosine kinase mutations in lung cancer identifies oncogenic extracellular domain mutations of ERBB2. *Proc. Natl. Acad. Sci. USA* **109**, 14476–14481 (2012).
- Geyer, C.E. *et al.* Lapatinib plus capecitabine for HER2-positive advanced breast cancer. *N. Engl. J. Med.* **355**, 2733–2743 (2006).
- Verma, S. *et al.* Trastuzumab emtansine for HER2-positive advanced breast cancer. *N. Engl. J. Med.* **367**, 1783–1791 (2012).
- Phillips, G.D. *et al.* Dual targeting of HER2-positive cancer with trastuzumab emtansine and pertuzumab: critical role for neuregulin blockade in antitumor response to combination therapy. *Clin. Cancer Res.* **20**, 456–468 (2014).
- Wilson, T.R. *et al.* Widespread potential for growth-factor-driven resistance to anticancer kinase inhibitors. *Nature* **487**, 505–509 (2012).
- Sergina, N.V. *et al.* Escape from HER-family tyrosine kinase inhibitor therapy by the kinase-inactive HER3. *Nature* **445**, 437–441 (2007).
- Chakrabarty, A., Sánchez, V., Kuba, M.G., Rinehart, C. & Arteaga, C.L. Feedback upregulation of HER3 (ErbB3) expression and activity attenuates antitumor effect of PI3K inhibitors. *Proc. Natl. Acad. Sci. USA* **109**, 2718–2723 (2012).
- Chandarlapaty, S. *et al.* AKT inhibition relieves feedback suppression of receptor tyrosine kinase expression and activity. *Cancer Cell* **19**, 58–71 (2011).
- Amin, D.N. *et al.* Resiliency and vulnerability in the HER2-HER3 tumorigenic driver. *Sci. Transl. Med.* **2**, 16ra7 (2010).
- Das, P.M. *et al.* Reactivation of epigenetically silenced HER4/ERBB4 results in apoptosis of breast tumor cells. *Oncogene* **29**, 5214–5219 (2010).

- Sartor, C.I. *et al.* Her4 mediates ligand-dependent antiproliferative and differentiation responses in human breast cancer cells. *Mol. Cell Biol.* **21**, 4265–4275 (2001).
- Aertgeerts, K. *et al.* Structural analysis of the mechanism of inhibition and allosteric activation of the kinase domain of HER2 protein. *J. Biol. Chem.* **286**, 18756–18765 (2011).
- Wood, E.R. *et al.* A unique structure for epidermal growth factor receptor bound to GW572016 (Lapatinib): relationships among protein conformation, inhibitor off-rate, and receptor activity in tumor cells. *Cancer Res.* **64**, 6652–6659 (2004).
- Littlefield, P. *et al.* Structural analysis of the EGFR/HER3 heterodimer reveals the molecular basis for activating HER3 mutations. *Sci. Signal.* **7**, ra114 (2014).
- Red Brewer, M. *et al.* The juxtamembrane region of the EGF receptor functions as an activation domain. *Mol. Cell* **34**, 641–651 (2009).
- Warmuth, M., Kim, S., Gu, X.-J., Xia, G. & Adrián, F. Ba/F3 cells and their use in kinase drug discovery. *Curr. Opin. Oncol.* **19**, 55–60 (2007).
- Jura, N. *et al.* Mechanism for activation of the EGF receptor catalytic domain by the juxtamembrane segment. *Cell* **137**, 1293–1307 (2009).
- Park, J.H., Liu, Y., Lemmon, M.A. & Radhakrishnan, R. Erlotinib binds both inactive and active conformations of the EGFR tyrosine kinase domain. *Biochem. J.* **448**, 417–423 (2012).
- Shi, F., Telesco, S.E., Liu, Y., Radhakrishnan, R. & Lemmon, M.A. ErbB3/HER3 intracellular domain is competent to bind ATP and catalyze autophosphorylation. *Proc. Natl. Acad. Sci. USA* **107**, 7692–7697 (2010).
- Jura, N., Shan, Y., Cao, X., Shaw, D.E. & Kuriyan, J. Structural analysis of the catalytically inactive kinase domain of the human EGF receptor 3. *Proc. Natl. Acad. Sci. USA* **106**, 21608–21613 (2009).
- Reyer, B.N. *et al.* Human breast cancer cells harboring a gatekeeper T798M mutation in HER2 overexpress EGFR ligands and are sensitive to dual inhibition of EGFR and HER2. *Clin. Cancer Res.* **19**, 5390–5401 (2013).
- Yoshida, T. *et al.* Identification and characterization of a novel chemotype MEK inhibitor able to alter the phosphorylation state of MEK1/2. *Oncotarget* **3**, 1533–1545 (2012).
- Adrián, F.J. *et al.* Allosteric inhibitors of Bcr-abl-dependent cell proliferation. *Nat. Chem. Biol.* **2**, 95–102 (2006).
- Scaltriti, M. *et al.* Expression of p95HER2, a truncated form of the HER2 receptor, and response to anti-HER2 therapies in breast cancer. *J. Natl. Cancer Inst.* **99**, 628–638 (2007).
- Chandarlapaty, S. *et al.* Inhibitors of HSP90 block p95-HER2 signaling in Trastuzumab-resistant tumors and suppress their growth. *Oncogene* **29**, 325–334 (2010).
- Sperinde, J. *et al.* Quantitation of p95HER2 in paraffin sections by using a p95-specific antibody and correlation with outcome in a cohort of trastuzumab-treated breast cancer patients. *Clin. Cancer Res.* **16**, 4226–4235 (2010).
- Sáez, R. *et al.* p95HER-2 predicts worse outcome in patients with HER-2-positive breast cancer. *Clin. Cancer Res.* **12**, 424–431 (2006).

Acknowledgments

We thank M. Hull, H. Nguyen, M. Wogan, J. Janes, P.G. Schultz and J. Roland from Calibr for technical assistance and helpful discussions. SK-BR-3 cells were a gift from S. Bandyopadhyay, and parental Ba/F3 cells were a gift from N. Shah (both at the University of California, San Francisco, San Francisco, California, USA). This work was supported in part by the Samuel Waxman Cancer Research Foundation (C.J.N., M.A.L. and K.M.S.), the U.S. National Institutes of Health (grant R01 GM109176-01A1 to K.M.S.), the Great Rivers Affiliate of the American Heart Association (predoctoral fellowship 11PRE7670020 to J.H.P.), and NIGMS (grant R01-GM099891 to M.A.L.).

Author contributions

C.J.N., M.A.L., W.S. and K.M.S. designed research; S.P. and W.S. performed the high-throughput screen and counter-screens; J.H.P. cocrystallized the 2-EGFR complex and performed the HER3 kinase assay; and C.J.N. conducted cell proliferation/growth and death experiments, western blots, chemical synthesis, creation of Ba/F3 cell lines, and *in vitro* HER2 and HER3 assays. All authors analyzed data and contributed to the writing of the manuscript.

Competing financial interests

The authors declare no competing financial interests.

Additional information

Any supplementary information, chemical compound information and source data are available in the [online version of the paper](#). Reprints and permissions information is available online at <http://www.nature.com/reprints/index.html>. Correspondence and requests for materials should be addressed to K.M.S. or W.S.

ONLINE METHODS

Cell culture and reagents. BT-474, MCF-7, NCI-H1781, CHL-1, and FaDu cells were purchased from ATCC; CW-2 cells were purchased from Riken Cell Bank; HEK293T cells were purchased from the UCSF cell culture facility; and EcoPack-293 cells were purchased from Clontech. SK-BR-3 cells were a gift from Dr. Sourav Bandyopadhyay (UCSF), and parental Ba/F3 cells were a gift from Dr. Neil Shah (UCSF). All cell lines were maintained at 37 °C and 5% CO₂. BT-474, NCI-H1781, CW-2, Axl⁺ Ba/F3, and 2YF/3EG Ba/F3 cells were maintained in RPMI 1640 media (Gibco) plus 10% FBS. MCF-7, CHL-1, FaDu, HEK293T, and EcoPack-293 cells were maintained in DMEM (Gibco) plus 10% FBS. SK-BR-3 cells were maintained in McCoy's 5A (Gibco) plus 10% FBS. Parental Ba/F3 cells were maintained in RPMI 1640 media plus 10% FBS supplemented with 10 ng/ml IL-3. 2YF/3wt, 2YF/3TM, 2YFTM/3wt, 2YFTM/3TM, 2YF-L755S/3wt, 2YF-YVMA/3wt, and 2YF-VC/3wt Ba/F3 cells were maintained in RPMI 1640 medium plus 10% FBS supplemented with 6.25 ng/ml NRG.

Lapatinib and TAK-285 were purchased from Selleckchem and were aliquoted and stored as 10 mM DMSO stocks at -20 °C. Anti-phospho-EGFR (Y1068) (cat. no. 3777), anti-EGFR (cat. no. 4267), anti-phospho-HER2 (Y1221/Y1222) (cat. no. 2243), anti-HER2 (cat. no. 2165), anti-phospho-HER3 (Y1289) (cat. no. 2842), anti-HER3 (cat. no. 12708), anti-HER4 (cat. no. 4795), anti-phospho-Akt (T308) (cat. no. 2965), anti-Akt (cat. no. 2920), anti-phospho-ERK (cat. no. 9101), anti-ERK (cat. no. 4695), anti-phospho-S6 (S240/244) (cat. no. 2215), anti-S6 (cat. no. 2217), anti-phospho-4-EBP1 (T37/46) (cat. no. 2855), anti-4EBP1 (cat. no. 9644), anti- α -tubulin (cat. no. 3873), and human neuregulin-1 (cat. no. 5218) were purchased from Cell Signaling Technology (CST). Mouse IL-3 (cat. no. PMC0034) was purchased from Gibco.

Cloning and Ba/F3 cell selection. Site-directed mutagenesis was carried out according to standard protocols on the human HER2 and HER3 sequences in pcDNA3.1. The desired constructs were Gibson-cloned into the pMSCV plasmid (Clontech) containing the gene for puromycin resistance (HER3, Axl) or for neomycin resistance (HER2)⁴⁴. The sequences of all constructs were confirmed with DNA sequencing. To produce virus, EcoPack-293 cells in a six-well plate were transfected with the desired pMSCV plasmid using lipofectamine LTX (Invitrogen) according to the manufacturer's protocol. Media was exchanged 8 h after transfection. 48 h after transfection the viral supernatant was filtered through a 0.2 μ m filter and added to one well of a six-well plate containing 2 \times 10⁶ Ba/F3 cells in 1 ml of RPMI media containing 40% FBS, 10 ng of IL-3, and 4 μ g of polybrene (Sigma). The cells were then centrifuged at 2,000g for 90 min at room temperature, placed back in the incubator for 24 h, and then added to a T-75 flask containing fresh RPMI 1640 media supplemented with 10 ng/ml of IL-3 and incubated for an additional 24 h.

For the 2YF/3wt cells, the parental cells were first transduced with HER3 according to the protocol above and were then spun down at 500g for 5 min and resuspended in media supplemented with 10 ng/ml IL-3 and 3 μ g/ml puromycin (Invitrogen). Cells were maintained in these conditions for 7 d, with passaging as required. After 7 d the cells were spun down, washed with fresh media, and then used for a subsequent round of transduction according to the protocol above with HER2YF virus. 48 h after the second transduction, the cells were resuspended in RPMI 1640 media containing 10 ng/ml IL-3 and 800 μ g/ml G418 (Invitrogen). The cells were maintained in these conditions for 7 d, with passaging as required. After 7 d the cells were spun down, washed with fresh media, and then suspended in media supplemented with 10 ng/ml of NRG. Cells were maintained in these conditions for 7 d to select for an NRG-dependent population of 2YF/3wt Ba/F3 cells that were then maintained as described above. The same protocol was used for the 2YF-L755S/3wt, 2YF-YVMA/3wt, and 2YF-VC/3wt cell lines using the indicated constructs.

For the HER2YF/3TM, HER2YFTM/3wt, and HER2YFTM/3TM Ba/F3 cell lines, we used an identical protocol with the exception that the populations were selected first for expression of the indicated HER2 construct (G418 resistance), and then for expression of the indicated HER3 construct (puromycin resistance).

HER2YF/3EG Ba/F3 cells were selected according to the protocol for the HER2YF/3TM Ba/F3 cells with the exception that no NRG was supplemented in the media during IL-3-independent selection.

For Axl⁺ cells, the transduced cells were spun down at 500g for 5 min and resuspended in media supplemented with 10 ng/ml IL-3 and 3 μ g/ml puromycin (Invitrogen). Cells were maintained in these conditions for 7 d, with passaging as required. After 7 d the cells were spun down, washed with fresh media, and then suspended in IL-3-free media. The cells were maintained in these conditions for 2 weeks to select for an IL-3-independent population of Axl⁺ driven cells.

Proliferation assays. For adherent cell lines, cells were plated onto opaque white 96-well plates (Greiner; 655083) and allowed to adhere overnight. The following day, media was changed to fresh media that contained either DMSO or the indicated concentration of drug plus NRG (50 ng/ml final concentration) as indicated. Plates were incubated at 37 °C for 72 h, and cell viability was read out using CellTiter-Glo assay (Promega) according to the manufacturer's protocol. For Ba/F3 cell proliferation, cells, drug dilution, and any necessary growth factors (10 ng/ml IL-3 or 6.25 ng/ml NRG) were combined in a well of a 96-well plate. Plates were incubated at 37 °C for 48 h, and proliferation was read out using CellTiter-Glo according to the manufacturer's protocol. For all normalized assays, proliferation was normalized to the DMSO control condition. All graphs were plotted in GraphPad Prism 6 and fit with a nonlinear regression of the log(inhibitor) versus response with a variable slope where shown. All graphs show averages (\pm s.d.) of biological triplicates, each performed in technical triplicate, unless otherwise noted.

Immunoblotting. Cells were grown in six-well plates and treated according to the indicated conditions, at which point the media was aspirated, cells were washed with 1 ml of cold PBS (which was then aspirated), and the plates were frozen at -80 °C. The frozen cells were thawed on the plates in a buffer containing 50 mM Tris, pH 7.5, 150 mM NaCl, 1 mM EDTA, and 1% Triton X-100 supplemented with 1 \times phosphatase (PhoSTOP, Roche) and 1 \times protease (complete-mini tablets, Roche) inhibitors. Lysates were scraped, transferred to Eppendorf tubes, and cleared by centrifugation at 20,000g for 20 min at 4 °C. The clarified lysates were transferred to chilled, clean tubes and normalized for protein concentration by Bradford assay (Bio-Rad). The normalized lysates were diluted with Laemmli loading buffer, and 10 μ g of total protein was run on a 4-12% gradient gel (Invitrogen), which was then transferred to 0.45 μ m nitrocellulose (Bio-Rad) and analyzed using the indicated primary antibodies according to the manufacturer's recommendations (1:1,000 antibody dilution). Primary antibodies were detected using IRDye secondary antibodies (Li-Cor) according to the manufacturer's recommendations and scanned on an Odyssey imager (Li-Cor). Scanned images were cropped and assembled in Adobe Illustrator 6.

For the HER3 immunoprecipitation, cells were treated the same as above but were lysed in a buffer containing 20 mM Tris, pH 7.5, 150 mM NaCl, 1 mM EDTA, and 1% Triton X-100 supplemented with 1 \times phosphatase (PhoSTOP, Roche) and 1 \times protease (complete-mini tablets, Roche) inhibitors. 1 mg of the total protein was immunoprecipitated with the HER3 antibody (CST, cat. no. 12708) at 4 °C overnight, followed by incubation with protein A beads (CST, cat. no. 8687) for 30 min at room temperature. The beads were washed three times with lysis buffer, eluted by boiling in 3 \times laemmli buffer, and analyzed by western blotting as detailed above.

High-throughput screening and analysis. For compound screening, 20 nL of 1 mM compound solutions in DMSO were transferred (Echo Labcyte) into white 1,536-well plates. Subsequently, cells were seeded in 5 μ l of growth medium (500 cells per well) using an automated plate filler (Kalypsys), resulting in a 4 μ M compound concentration. Each assay plate included neutral (DMSO only) and inhibitor (lapatinib) control wells. CellTiter-Glo Reagent (Promega, 2 μ l per well) was added 2 d later. Luminescence signal was read after 10 min using an automated plate reader (ViewLux or Envision, PerkinElmer). The data were analyzed using the Genedata Screener software, normalized by neutral control. The percentage inhibition for each tested compound was calculated on a per-plate basis, and all compounds that showed >50% inhibition of the luminescence signal as compared with the DMSO control were picked as primary hits for triplicate confirmation. Hits confirmed with >50% inhibition in two out of the three replicates were subsequently assayed in parental Ba/F3 cells

in the presence of IL-3, and nontoxic hits (<30% inhibition in parental cells) were further assayed in dose response in 2YF/3wt cells in the presence of NRG, parental BaF3 cells in the presence of IL-3, and BaF3 Axl⁺ cells in order to identify hits that selectively inhibit the 2YF/3wt cells in the presence of NRG.

In vitro kinome screen. *In vitro* profiling of **2** at 100 nM and 1 μ M and of **3** at 1 μ M was conducted by Nanosyn.

Real-time cell proliferation assay. CHL-1 cells were plated in clear-bottom black 96-well plates (Corning; 3904) and allowed to adhere overnight. The following day, media was changed to fresh media that contained either DMSO or compound. Confluence was measured every 2 h for 96 h using two bright-field images per well taken on an InCuCyte Zoom (Essen BioScience). Data were graphed in GraphPad Prism 6 and are averages of biological duplicates, each performed in technical triplicate.

In vitro HER2 kinase assay. *In vitro* kinase assays with the HER2 kinase domain (SignalChem) were performed in triplicate as follows. To 9 μ L of a 2.5 \times solution of kinase and substrate in reaction buffer, we added 3 μ L of a 5 \times DMSO or inhibitor dilution in 10% DMSO:water. The inhibitor-kinase solution was incubated at room temperature for 10 min. The kinase assay was initiated by the addition of 3 μ L of a 5 \times solution of ATP and ran for 15 min. The final reaction conditions were 50 mM Tris, pH 7.4, 5 mM MnCl₂, 0.01% Tween-20, 2 mM DTT, 100 μ M E₄Y substrate (SignalChem), 15 nM HER2, 2% DMSO, 50 μ M ATP, and 1 μ Ci γ ³²P-ATP. After 15 min, 3 μ L of each reaction was pipetted onto phosphocellulose sheets (P81, Whatman) and allowed to dry. The sheets were then washed four times for 5 min each time with a solution of 0.5% phosphoric acid, dried, and exposed to a phosphor screen overnight. Phosphorimaging was conducted on a Typhoon 9500, and image intensities were quantified in ImageQuant 5.2, normalized to the DMSO control, and plotted in GraphPad Prism 6.

HER3 thermofluor assay. The HER3 gatekeeper mutation (T787M) was introduced into the HER3 tyrosine kinase domain in the pFastBac plasmid using standard protocols. Both wild-type and T787M HER3 were purified according to previously published protocols³⁵. Thermofluor reactions were performed in duplicate and set up as follows: 1 μ L of an inhibitor or DMSO dilution in 40% DMSO:water was added to 19 μ L of the HER3 kinase domain in reaction buffer. The final reaction solution contained 100 mM MOPS, 200 mM NaCl, 5% glycerol, 5 mM MgCl₂, 0.1 mM DTT, 5 \times SYPRO Orange, 2 μ M kinase, 2% DMSO, and 20 μ M inhibitor in the wells of a 96-well, low-profile, white PCR plate (USA Scientific). The solution was pipetted up and down to mix, sealed with TempAssure clear PCR flat caps (USA Scientific), centrifuged at 500g for 30 s, and heated in a Stratagene Mx3005P RT-PCR machine from 25 $^{\circ}$ C to 95 $^{\circ}$ C in 0.5 $^{\circ}$ C increments every 30 s after an initial incubation at 25 $^{\circ}$ C for 10 min. Fluorescence was measured at the end of each 30-s period with an excitation wavelength of 492 nm and an emission wavelength of 610 nm. To obtain the melting temperature, we normalized fluorescent signals to the maximum fluorescent signal for that well. Values after the well had reached a maximum signal were discarded, and the signals were fit to the Boltzmann equation in GraphPad Prism 6. ΔT_m was calculated as the difference in melting temperature between the compound-treated kinase and the DMSO control.

Transfected HER2 kinase activity. The HER2 gatekeeper mutation (T798M) was introduced into the *HER2* gene in pcDNA3.1 using standard protocols. HEK293T cells were transfected with the indicated pcDNA3.1 constructs of HER2 using Lipofectamine LTX according to the manufacturer's protocol. 24 h after transfection the media was exchanged for fresh drug-containing

media. After 1 h of drug treatment, the cells were processed for immunoblots according to the protocol outlined above.

Cell death assay. Cells were plated in clear-bottom, black, 96-well plates (Corning; 3904) and allowed to adhere overnight. The following day the media was changed to fresh media that contained 1 \times concentration of CellTox green (Promega) and either DMSO or the indicated concentration of drug \pm NRG (50 ng/ml). Cells were allowed to grow for 72 h, after which the number of dead cells was measured using the InCuCyte Zoom system. Immediately after the 72-h read, 5 μ L of 1.25% Triton X-100 was added to each well and wells were incubated at 37 $^{\circ}$ C for 30 min to lyse all cells, which were then counted by the InCuCyte. We calculated the percent cell death by dividing the number of dead cells counted at 72 h by the number of total DNA-containing cells after the detergent treatment. Values are the average of biological triplicates each performed in technical triplicate and were plotted in GraphPad Prism 6.

Crystallization and structure determination. Expression and purification of EGFR⁶⁷²⁻⁹⁹⁸ V924R (EGFR TKD V924R) were performed exactly as previously described³⁴. For the structure of EGFR TKD V924R bound to **2**, EGFR TKD protein was concentrated to 8 mg/ml in 20 mM Tris-HCl, pH 8.0, containing 150 mM NaCl and 2 mM DTT. Protein was cocrystallized with an excess of **2** (1:2 molar ratio) in a reservoir solution of 1.34 M ammonium sulfate, 1.34% (vol/vol) PEG 400, and 0.1 M sodium acetate/acetic acid, pH 5.5, in the hanging drop at 21 $^{\circ}$ C. Crystals were cryo-protected in reservoir solution with added 20% (wt/vol) glycerol and flash-frozen in liquid nitrogen. Diffraction data were collected at beamline 23ID-B of GM/CA@APS (Advanced Photon Source), where crystals diffracted to 3.3 \AA , and were processed using HKL2000 (see **Supplementary Table 2**). The structure was solved by molecular replacement using Phaser with the active EGFR (wild-type) TKD structure (PDB 1M17) as an initial search model. Repeated cycles of manual building/rebuilding using Coot were alternated with rounds of refinement using REFMAC and PHENIX, plus composite omit maps calculated using PHENIX. Coordinates, parameter files, and molecular topology of **2** were generated by PRODRG⁴⁵. Data collection and refinement statistics are shown in **Supplementary Table 4**, and structural figures were generated with PyMOL.

HER3 autophosphorylation assay. ErbB3-ICD⁶⁶⁵⁻¹³²³ wild-type expression and purification were performed exactly as previously described³⁵. To monitor the change in autophosphorylation, we incubated 1 μ M ErbB3-ICD⁶⁶⁵⁻¹³²³ protein with inhibitors (varying concentrations noted in figures) and DOGS-Ni-NTA (prepared as described in ref. 4) in 100 mM MOPS, pH 7.4, containing 200 mM NaCl, divalent cations (2 mM MnCl₂ plus 5 mM MgCl₂), 5% glycerol, 0.1 mM DTT, and 200 μ M ATP for 1 h at 25 $^{\circ}$ C, and the reactions were stopped by addition of 50 mM EDTA and SDS-PAGE gel-loading buffer for rapid qualitative comparison of autophosphorylation by SDS-PAGE and immunoblotting with anti-phosphotyrosine (pY20; Enzo Life Sciences, SA240, 1:1,000) and anti-(His)₅ (Qiagen, 34660, 1:1,000).

Pharmacokinetic evaluation of 3. Pharmacokinetic profiling of compound **3** was performed by Biotranex.

General methods for chemistry. Full experimental details and characterization data for all new compounds are included in the **Supplementary Note**.

- Gibson, D.G. *et al.* Enzymatic assembly of DNA molecules up to several hundred kilobases. *Nat. Methods* **6**, 343–345 (2009).
- Schüttelkopf, A.W. & van Aalten, D.M.F. PRODRG: a tool for high-throughput crystallography of protein-ligand complexes. *Acta Crystallogr. D Biol. Crystallogr.* **60**, 1355–1363 (2004).

Reproduced with permission of the copyright owner. Further reproduction prohibited without permission.